

# Adjust the electrochemical performances of graphene oxide nanosheets-loaded poly(3,4-ethylenedioxythiophene) composites for supercapacitors with ultralong cycle life

Haihan Zhou<sup>1</sup> · Hua-Jin Zhai<sup>1</sup> · Gaoyi Han<sup>1</sup>

Received: 12 September 2015 / Accepted: 15 November 2015 / Published online: 20 November 2015  
© Springer Science+Business Media New York 2015

**Abstract** The graphene oxide nanosheets-loaded poly(3,4-ethylenedioxythiophene) (GO/PEDOT) intercalation composites have been fabricated successfully with a facile electrochemical method. The varying deposition time was implemented to investigate the effect of loading amount on electrochemical behavior of the composites. The GO/PEDOT nanocomposites showed the superior capacitive behaviors, and achieved a high areal capacitance of  $66.3 \text{ mF cm}^{-2}$  at  $10 \text{ mV s}^{-1}$  cyclic voltammetry (CV) scan. The scanning electron microscope characterization indicated different deposition time would significantly affected the curly sheet-like morphology of composites. Moreover, the composite films prepared with longer deposition time exhibited relatively lower capacitance value at the fast CV scan. Meanwhile, the galvanostatic charge/discharge tests indicated moderate deposition time was more suitable for the fast charge/discharge. In particular, a stability test of 20,000 CV cycles revealed the composites had the ultra long cycle life. We consider that the highly stable GO/PEDOT nanocomposites with superior capacitive behaviors are very promising for high-performance electrochemical energy storage.

## 1 Introduction

Electrochemical capacitors (also called supercapacitors), as one kind of novel charge-storage devices, possess higher power density and longer cycle life than the secondary batteries, and larger energy density than the conventional capacitors. They have been extensively studied nowadays and are being employed in various applications range from portable electronic devices to hybrid electric vehicles, back-up power supplies, etc. [1–8].

The energy storage mechanism in electrochemical capacitors is usually Faradic and electrical double-layer. Based on the corresponding charge storage mechanism, supercapacitors can be divided into redox supercapacitors and electrical double-layer capacitors (EDLCs) [9–11]. In general, carbon materials (activated carbon, carbon nanotubes, and graphene, etc.) are employed as the electrode materials for the EDLCs, while the redox supercapacitors use transitional metal oxides and conducting polymers. However, EDLCs is due to the electrosorption of ions on porous carbon electrodes, consequently limited energy density, pseudo-capacitors provide higher energy densities but usually suffer from shorter cyclic lifetimes [12–15]. Considering these factors, considerable attention has been devoted to developing hybrid materials combining the advantages of EDLCs and redox supercapacitors to obtain high-performance capacitive electrode materials [16–19]. Moreover, recent research efforts have also been focused on improving the energy density of supercapacitors by exploring new electrode materials [20–22].

Due to exhibiting not only a high conductivity but also an unusual stability in the oxidized state compared to other types of conducting polymers (CPs), poly(3,4-ethylenedioxythiophene) (PEDOT) has attracted a lot of attention of many researchers for the electrode material of

✉ Haihan Zhou  
hhzhou@sxu.edu.cn

<sup>1</sup> Institute of Molecular Science, Key Laboratory of Materials for Energy Conversion and Storage of Shanxi Province, Key Laboratory of Chemical Biology and Molecular Engineering of Education Ministry, Shanxi University, Taiyuan 030006, China

supercapacitors [23, 24]. In addition, owing to a low fabrication cost and an environmentally friendly nature, graphene oxide (GO) can be easily synthesized from natural graphite and form stable dispersions in water, which is derived from the charge highly oxidized structure with a large number of oxygen containing functional groups (alkoxy, epoxy, carbonyl, and carboxyl groups) on the surface of GO sheets [25, 26]. To combine advantages of double layer capacitance and pseudocapacitance, some researches have been devoted to developing the composites of CPs and GO nanosheets for supercapacitor electrodes. However, these materials were usually prepared with complicated multiple-step procedures or using the chemical oxidative polymerization [27–29]. Compared with chemical oxidative polymerization, electrochemical polymerization shows the advantages that the films can be deposited directly on the electrode substrates, and the film thickness can easily be controlled and the films are free from impurities (e.g. the oxidant and its reaction products). Fortunately, the anionic character of GO makes it possible to act as dopant during electrochemical polymerization of conducting polymers to form CPs/GO composite films deposited on a variety of electrode substrates. Currently, some preliminary studies have revealed the feasibility of electrochemical synthesis for the composites consist of CPs and GO [30–32], but the capacitive behavior remains unsatisfactory, especially the cycle stability of composites was not studied, it is probably related to the system and parameters prepared. So it is a big challenge to synthesize GO/PEDOT composites as electrode materials possessing the high capacitance, superior rate capability, and cycle stability for supercapacitors. What's more, almost all the related researches focus on the mass specific capacitance of electrode materials, up to date, few works has been reported on the investigation of areal capacitance of conducting polymers/GO composites. For applications such as small scale electronics and stationary energy storage devices where areal capacitance is a better indicator of the supercapacitor performance than mass specific capacitance although the mass specific capacitance has always been used in the literature for comparison of the supercapacitor performance [33, 34], so this study would focus on the areal capacitance of composite films.

Here GO/PEDOT composites have been prepared by a facile electrochemical polymerization method. The compositions and morphology as well as the structures of the composite films were studied with Fourier transform infrared spectroscopy (FT-IR), Transmission electron microscopy (TEM), X-ray diffraction (XRD), and scan electron microscope (SEM). The influence of deposition time (i.e. deposition amount) on the electrochemical performances of the GO/PEDOT composites was investigated with cyclic voltammetry (CV), galvanostatic charge/discharge (GCD)

measurements, and electrochemical impedance spectroscopy (EIS), finally an ultralong cycle stability test was performed.

## 2 Experimental

### 2.1 Materials

Natural graphite powder (325 mesh) was purchased from Tianjin Guangfu Research Institute. 3, 4-ethylene-dioxythiophene (EDOT, Ourchem<sup>®</sup>, 99 %) was obtained from Sinopharm Chemical Reagent Co. Ltd (Shanghai, China). Fluorine-doped tin oxide (FTO,  $8 \Omega/\square$ ) conducting glasses were purchased from Dalian Heptachroma Solar-Tech, the conductive areas ( $1 \text{ cm} \times 1 \text{ cm}$ ) were exposed as the substrate for electrochemical deposition. The glasses were ultrasonically cleaned in acetone and deionized water successively prior to use.

### 2.2 Electrode preparation

GO was prepared by oxidizing the natural graphite powder and subsequent exfoliation by ultrasonication according to the method reported in literatures [35, 36]. The obtained GO aqueous dispersion was treated with freeze drying and preserved at the room temperature. The GO/PEDOT composite films electrodes were prepared by electrochemical polymerization, and the polymerization solution did not contain any other supporting electrolyte but only GO serving as a weak electrolyte. For a standard procedure of polymerization, an aqueous solution containing  $2 \text{ mg mL}^{-1}$  GO and 0.01 M EDOT monomer was dispersed under ultrasonication for about 20 min to form a homogenous colloidal solution. Subsequently, GO/PEDOT films were electrodeposited onto the FTO conducting glasses with a galvanostatic mode, in which a current of  $1.0 \text{ mA cm}^{-2}$  was applied, the varying deposition time including 10, 20, 30, and 40 min is carried out, and the as-prepared composite films are named as GO/PEDOT-10, GO/PEDOT-20, GO/PEDOT-30, and GO/PEDOT-40, respectively. It should be noted that the FTO conducting glasses were used as the substrate for electrodeposition because their high conductivity and were usually used in the dye-sensitised solar cell (DSSC). After that, the composite films-deposited glasses were washed with adequate deionized water to remove the unreacted substance. In the process of deposition, the cleaned FTO conducting glasses were fixed in the two-electrode system with a large-area Pt sheet acting as the counter electrode and pseudo-reference electrode. In addition, the pure PEDOT films were prepared from solutions containing 0.01 M EDOT monomer and 0.1 M KCl with the same deposition procedure for FT-IR test.

### 2.3 Morphology

The SEM images of the composite films were obtained with a field emission scanning electron microscope (JSM-6701F, JEOL). The morphologies of GO and GO/PEDOT composites were observed using a high-resolution transmission electron microscopy (JEM-2100, JEOL).

### 2.4 Composition and structural characterization

The test samples were scraped from the surface of FTO conducting glasses with deposited films for the thickness, FT-IR, and XRD tests. FT-IR spectra were tested with a Bruker Tensor 27 FT-IR spectrometer, in which all samples were prepared by potassium bromide tableting. The XRD patterns of the samples were obtained on a Bruker D8 Advance X-ray diffraction meter with Cu K $\alpha$  radiation and graphite monochromator at the scan speed of 5° min<sup>-1</sup> with a step size of 0.02°.

### 2.5 Electrochemical tests

The capacitor cells for electrochemical tests were assembled with two pieces of composite films-deposited FTO glasses (one oxidized and one reduced) as the two electrodes, a filter paper soaked with 1.0 M KCl electrolyte was used as the separator, the conducting glass itself served as the current collector. All the electrochemical tests were made using an electrochemical workstation (CHI 660B, Chenhua, China) with the two-electrode system. Thereinto, the CV measurements were performed between potentials of -0.5 to 0.5 V, and the scan rates range from 5 to 1000 mV s<sup>-1</sup>. The GCD tests were carried out at varying current density with the cutoff voltage of -0.5 and 0.5 V. The EIS were measured using 5 mV (rms) AC sinusoid signal at a frequency range from 100 k to 0.01 Hz at the open circuit potential. During all the electrochemical tests, the capacitor cells were wrapped with preservative films to prevent the volatilization of electrolyte.

Focus on the applications such as stationary energy storage devices and small scale electronics, areal capacitance is a better indicator of the performance of electrochemical capacitors than mass specific capacitance [37, 38], so this research concentrates on the areal capacitance of electrodes. On the basis of the CV curves, the areal capacitance ( $C_s$ ) value of a single electrode can be calculated according to the following Eq. (1):

$$C_s = \left( \int idV \right) / (S \times \Delta V \times \nu) \quad (1)$$

where  $C_s$  is the areal capacitance in F cm<sup>-2</sup>,  $\int idV$  the integrated area of the CV curve,  $S$  the surface area of active materials in the single electrode in cm<sup>2</sup> and it is fixed at

1 cm<sup>2</sup> in this study,  $\Delta V$  the scanning potential window in V and  $\nu$  the scan rate in V s<sup>-1</sup>.

The galvanostatic charge/discharge measurements by chronopotentiometry were also performed to evaluate the areal capacitance of the nanocomposites using the Eq. (2):

$$C_s = (2 \times i \times t) / (S \times \Delta V) \quad (2)$$

where  $C_s$  is the areal capacitance in F cm<sup>-2</sup>,  $i$  the discharge current in A,  $t$  the discharge time in s,  $S$  the surface area of the active materials on the single electrode in cm<sup>2</sup> and  $\Delta V$  the scan potential window in V.

## 3 Results and discussion

### 3.1 Compositions, structures, and morphology

FT-IR and XRD tests were carried out to determine the compositions and structures of the GO/PEDOT composites, and the FT-IR spectra of GO, PEDOT, and GO/PEDOT are exhibited in Fig. 1a. For the GO spectrum, the peak at 1703 cm<sup>-1</sup> can be ascribed to the C=O stretching of carbonyl. The peaks at 1413 and 1235 cm<sup>-1</sup> originate from the O-H deformation and C-OH stretching vibration, and the peak at 1055 cm<sup>-1</sup> is the characteristic peak for epoxide group [39]. In the spectrum of pure PEDOT spectrum, the quinoid structure and stretching modes of C-C and C=C in the thiophene ring cause the vibrations around 1350 and 1518 cm<sup>-1</sup>, respectively [40]. Peaks at 1058, 1089, 1144, and 1203 cm<sup>-1</sup> are attributed to the stretching of the C-O-C bond in the ethylenedioxy group [41]. Vibration at 926 cm<sup>-1</sup> is related with the ethylenedioxy ring deformation mode [42], and the modes of vibration for the C-S bond in the thiophene ring are observed at 692, 841 and 980 cm<sup>-1</sup> [41, 43]. As to GO/PEDOT spectrum, it shows the characteristic peaks of PEDOT, and the only difference is that the vibration band ascribed to C-C stretching in the thiophene ring from GO/PEDOT composites show a redshift from 1350 to 1332 cm<sup>-1</sup> (marked with red). This is caused by the electrostatic interaction between the PEDOT cations and the GO anions, also the  $\pi$ - $\pi$  interactions and hydrogen bonding between the thiophene rings and GO layers. In addition, that the GO bands are detected scarcely in the GO/PEDOT spectrum is probably due to either too weak or overlapped with the characteristic peaks of PEDOT.

In the process of electrochemical polymerization, the anionic GO not only acts as the counter-ions for polymerization of EDOT monomer but also serves as the substrate for the adhesion and intercalation of PEDOT particles. The XRD patterns of GO, PEDOT, and GO/PEDOT composites are shown in Fig. 1b. We can see that GO pattern reveals an intense, sharp peak at  $2\theta = 10.9^\circ$ ,

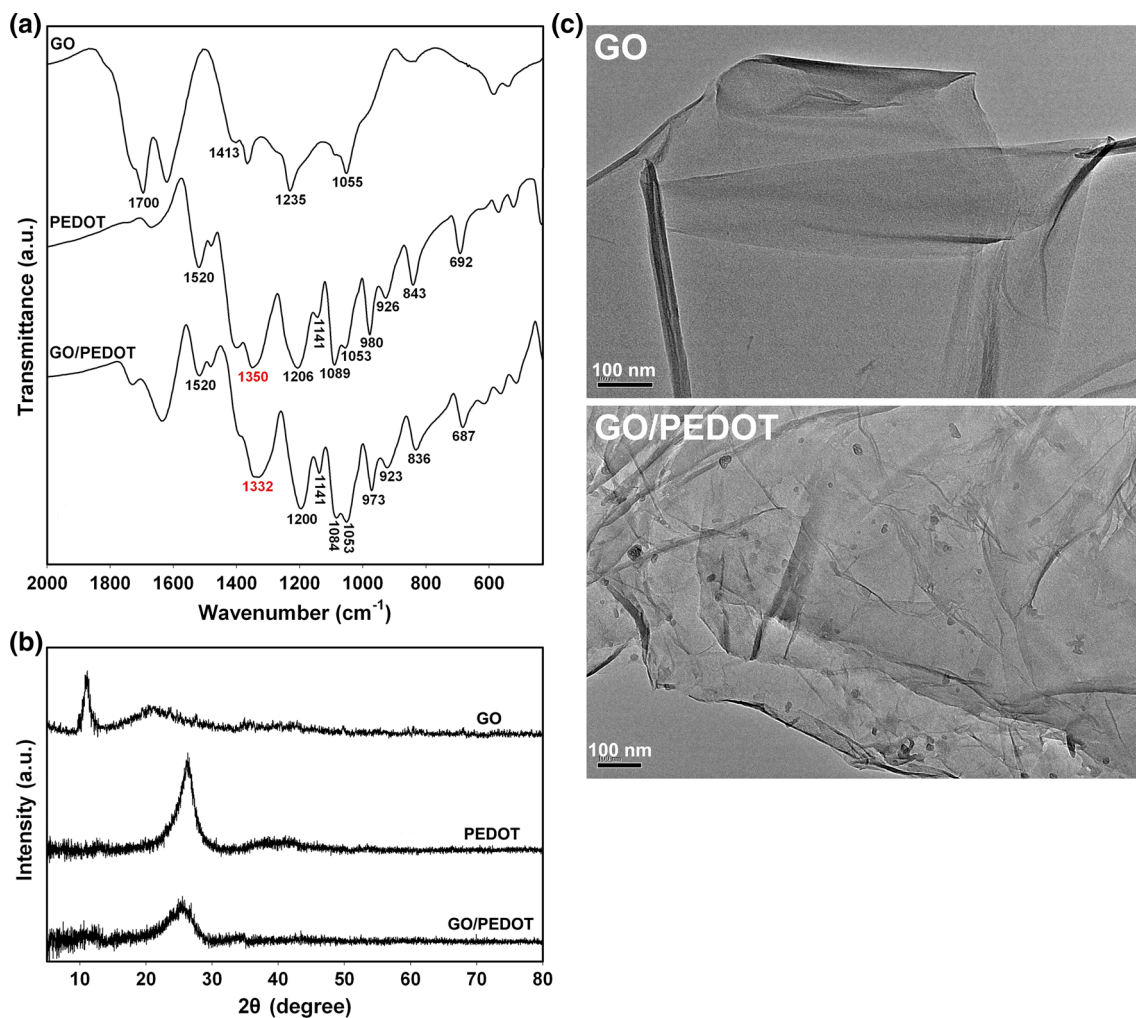


**Fig. 1** **a** FT-IR spectra of GO, PEDOT, and GO/PEDOT composites; **b** XRD patterns of GO, PEDOT, and GO/PEDOT composites; **c** TEM images of GO and GO/PEDOT composites

the calculation by Bragg equation indicates the GO sheets have an interplanar spacing ( $d$ -spacing) of 0.81 nm, which is larger than the 0.335 nm for pristine graphite ( $2\theta = 26.6^\circ$ ) resulting from the introduction of oxygenated functional groups [44]. In addition, the broad peak at  $21.4^\circ$  can be attributed to the aggregations of GO sheets [45]. In the PEDOT pattern, the broad diffraction peak at  $2\theta = 26^\circ$  indicates that PEDOT is amorphous in nature [46]. For the GO/PEDOT composites, the only broad peak located at  $26^\circ$  derived from the diffraction peak of PEDOT appears, while the peaks for GO almost disappear, indicating the PEDOT particles intercalated between the GO nanosheets increase the  $d$ -spacing of the layered GO, demonstrating the formation of GO/PEDOT intercalation nanocomposites.

With the purpose of observing the composite morphology of GO and GO/PEDOT, TEM characterization was performed and the images are shown in Fig. 1c. It can be

observed that the GO shows the sheet-like morphology with smooth and curly edge, and the nanosheets have a large surface area. Compared to the GO, GO/PEDOT composites display the overlapped structure with multi-layer GO nanosheets and the wrinkle of GO decreases, which in accordance with the previous report that the wrinkle of GO would decrease with the increase of layers for GO nanosheets [47]. A careful inspection of the nanostructures of GO/PEDOT composites suggests that PEDOT particles are decorated dispersedly on the surface and intercalate the GO sheets. TEM characterization further reveals that PEDOT coated on the GO surface and filled between the GO nanosheets to form the intercalated composite nanostructures. This nanostructures will be beneficial to increase the electroactive area and combine the advantages of EDLCs and redox supercapacitors derived from GO and PEDOT.

### 3.2 Capacitive behavior of GO/PEDOT nanocomposites

In this research, the capacitive behavior was investigated with two-electrode system, which is a good estimation of performance for supercapacitor electrodes [48]. CV and GCD tests of GO/PEDOT-10 electrodes were carried out to investigate the capacitive behavior of the composites. We can see from Fig. 2a that the curves at varying CV scan rates do not show obvious redox peaks in the whole CV scan process, which indicates that the electrode was charged and discharged at a pseudo-constant rate, it is because that the capacitor was assembled by two identical electrodes, one was oxidized and the other reduced during the scan, resulting in the oxidation/reduction peaks of PEDOT unobvious. The rectangular-like CV curves with the almost symmetric I-E responses can be observed at all scan rates range from 10 to 200 mV s<sup>-1</sup> and the obvious

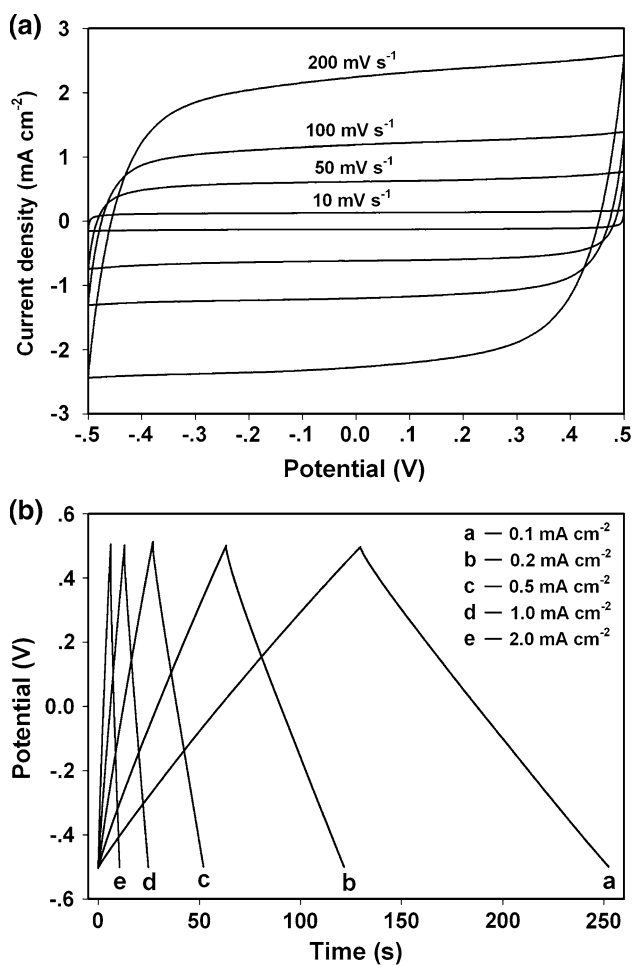


**Fig. 2** a CV curves at varying scan rates rang from 10 to 200 mV s<sup>-1</sup> and b GCD curves at different GCD current densities rang from 0.1 to 2 mA cm<sup>-2</sup> of the capacitor cells assembled by GO/PEDOT-10 composite films-deposited electrodes

increase of current with scan rates, indicating that the GO/PEDOT nanocomposites have superior rate capability.

The GCD tests were also carried out at different current densities range from 0.1 to 1 mA cm<sup>-2</sup> and the plots are exhibited in Fig. 2b. In the process of charge/discharge, the following electrochemical redox reaction has taken place: PEDOT<sup>+</sup>/GO<sup>-</sup> + K<sup>+</sup> + e<sup>-</sup> ↔ PEDOT<sup>0</sup>/GO<sup>-</sup>/K<sup>+</sup>. With a fully charged state, the anodic process was neutral as a result of the PEDOT did not have n-doping ability, while the cathodic process was the fully oxidized state and charge neutrality was kept by the GO<sup>-</sup> anions. When the discharge happened, the PEDOT in the cathodic process was reduced and the anode oxidized, and the counter-ions ejected from the cathode were inserted in the anode to keep charge neutrality [49]. It can be seen from Fig. 2b that the charging curves at different current densities are nearly symmetric to their discharging parts, in addition, the areal capacitance of the GO/PEDOT composites reach 24.6 mF cm<sup>-2</sup> at 0.1 mA cm<sup>-2</sup>, when the current density increases to 2 mA cm<sup>-2</sup>, the areal capacitance is 17.6 mF cm<sup>-2</sup>, retaining ~72 % of that at 0.1 mA cm<sup>-2</sup>. These further indicate the composites have superior rate capability.

### 3.3 Effect of deposition time on the electrochemical performance

The previous investigations indicated the areal capacitance can be increased by adding the loading amount per unit area of electroactive materials on the electrode [50]. Fortunately, the loading amount of the electroactive materials on the electrodes with electrochemical deposition can be adjusted by changing the deposition time. In this research, the varying deposition time including 10, 20, 30, and 40 min was made and the electrochemical performance of nanocomposites obtained was compared. Thereinto, the thickness of obtained GO/PEDOT-10, GO/PEDOT-20, GO/PEDOT-30, and GO/PEDOT-40 composite films is around 4, 7.5, 10, and 12.5 μm, and their mass is 0.48, 0.92, 1.29, and 1.68 mg, respectively. The surface morphology is an important feature to affect the performance of electrode materials used for electrochemical capacitors. Figure 3 shows the SEM images of the four types of films, we can see that the composites prepared by electropolymerization are highly loose and consist of two-dimensional nanosheets interconnecting with each other, and all the four types of films show the curly sheet-like morphology. However, a significant change can be also observed from Fig. 3 and its inset is that the sheets become larger curly size with the adding of deposition time, and the GO/PEDOT-40 films show the maximum aggregation. The results of SEM characterization suggest that the morphology of the GO/PEDOT nanocomposites is affected

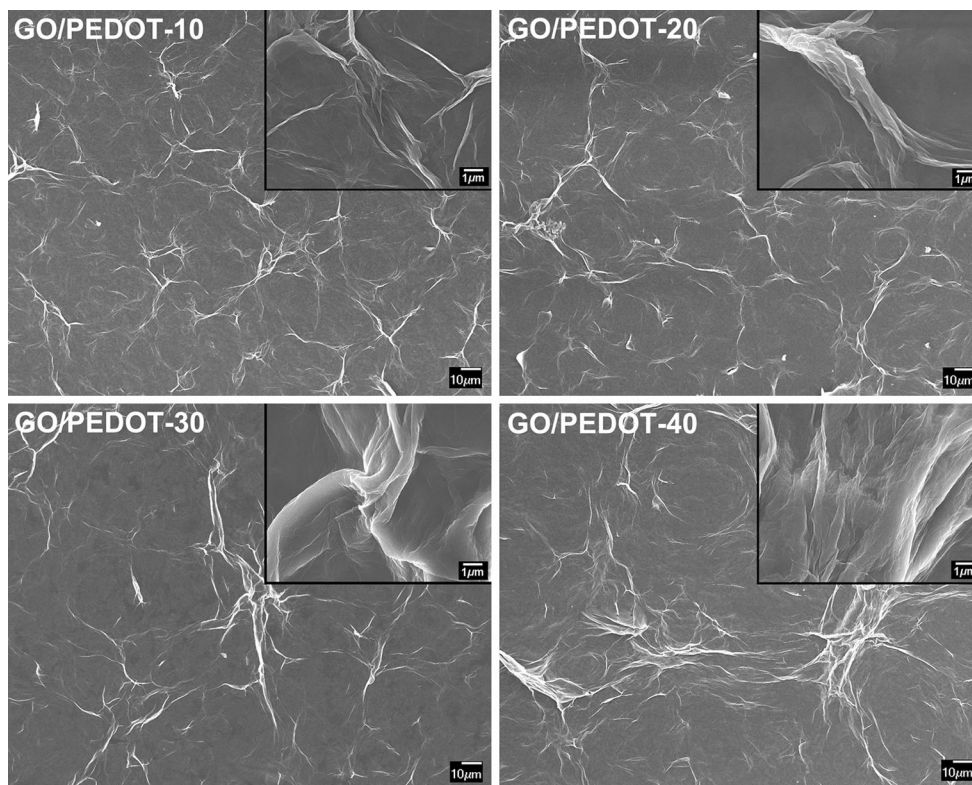


**Fig. 3** SEM images of GO/PEDOT composite films with different deposition time. The insets in the upper right are the corresponding SEM images at high magnification

obviously by the deposition time, longer deposition time would result in larger curly sheets.

The dependence of the areal capacitance on varying CV scan rate for the GO/PEDOT electrodes with varying deposition time is shown in Fig. 4. It can be observed that GO/PEDOT-40 shows the most inclined curve while GO/

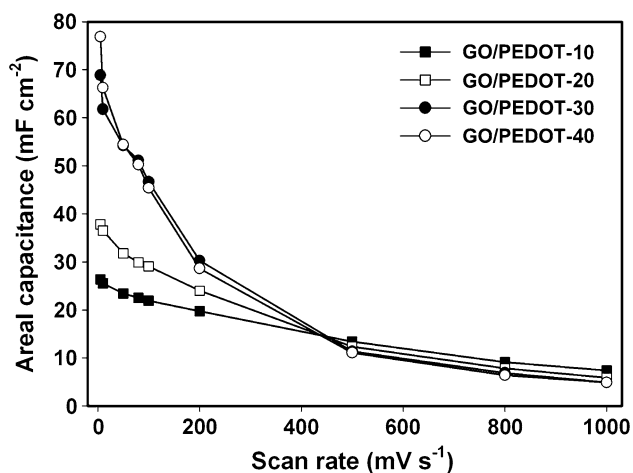


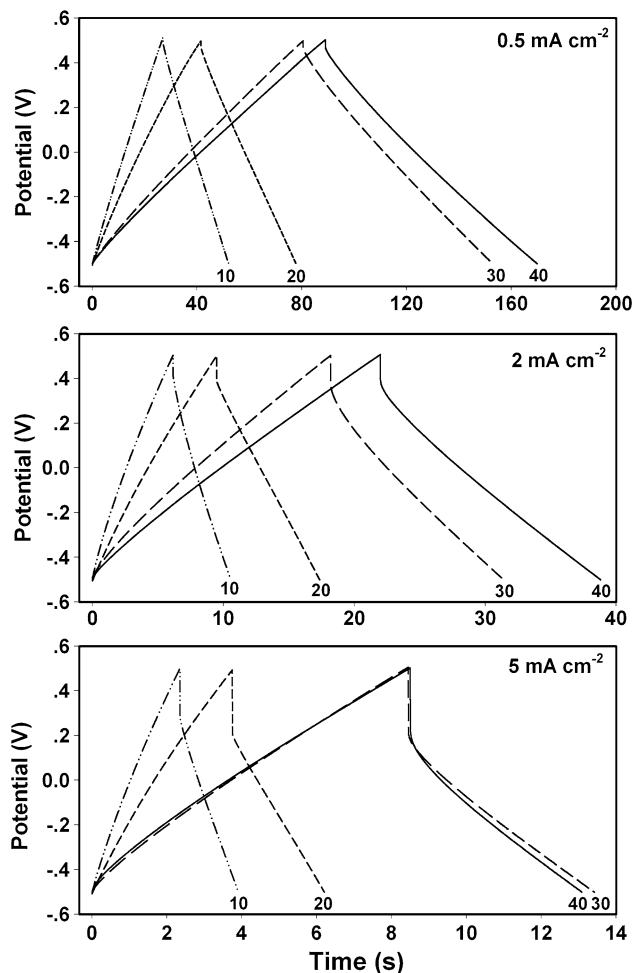
**Fig. 4** Areal capacitance versus CV scan rate plots for GO/PEDOT composite films electrodes with different deposition time

PEDOT-10 presents the smoothest curve, indicating the CV scan rate has a smaller effect on the areal capacitance for the relatively thinner composite films. The further observation in Fig. 4 reveals that areal capacitance increases as the adding of deposition time at the relatively low CV scan rates range from 5 to 50  $\text{mV s}^{-1}$ . The highest areal capacitance of  $76.9 \text{ mF cm}^{-2}$  is obtained for the GO/PEDOT-40 composite films at  $5 \text{ mV s}^{-1}$  and  $66.3 \text{ mF cm}^{-2}$  at  $10 \text{ mV s}^{-1}$ , which are higher than  $25 \text{ mF cm}^{-2}$  at  $5 \text{ mV s}^{-1}$  for PANI/graphite oxide composites and  $64.6 \text{ mF cm}^{-2}$  at  $10 \text{ mV s}^{-1}$  for  $\text{TiO}_2/\text{PPy}$  nanowires reported previously [38, 51]. However, as the further increases of CV scan rate, the gap of areal capacitance among the four types of composite films shows an obvious trend of decrease. When the scan rate rises to 500 as far as  $1000 \text{ mV s}^{-1}$ , the areal capacitance is nearly independent with the deposition time, nevertheless, GO/PEDOT-10 shows the relatively highest capacitance value, while GO/PEDOT-40 exhibits the relatively lowest capacitance value. These results can be attributed to the following reasons: (1) At the slow CV scan rate, the ions from the electrolyte have sufficient time to diffuse into the composite films, so the electroactive materials on the electrode can be used adequately, and then more active materials would result in larger areal capacitance. (2) As

the increase of scan rate, the ions from electrolyte have no enough time to diffuse, leading to only part of active materials can be utilized, in addition, thicker films would result in larger diffusion resistance of electrolyte ions and increase electron transport resistance, so the gap of areal capacitance among the four types of composite films gradually decreases. Especially, when the scan rate became faster than  $500 \text{ mV s}^{-1}$ , the only few active materials was used in the scan, so all the electrodes of varying deposition time exhibit the similar capacitance value. (3) Combining with the SEM characterization results, longer deposition time exhibits the morphology of larger aggregation size for curly sheets, which leads to smaller electrochemical surface and also not facilitate the diffuse of ions from electrolyte within the composite films, so the GO/PEDOT-40 shows the relatively lowest capacitance value at the fast CV scan although it has the most electroactive materials.

In order to further investigate the effect of deposition time on the capacitive behavior for the composite films, the GCD tests were performed. Figure 5 shows the GCD curves of supercapacitor cells assembled by four types of GO/PEDOT composite electrodes at different current densities including  $0.5, 2, \text{ and } 5 \text{ mA cm}^{-2}$ , and the corresponding discharge time and areal capacitance obtained from the GCD curves are listed in Table 1. In accordance with the CV tests, the discharge time increases as the adding of deposition time at the relatively low GCD current densities including  $0.5 \text{ and } 2 \text{ mA cm}^{-2}$ , GO/PEDOT-40 exhibits the highest areal capacitance, nevertheless, when the GCD current density increases to  $5 \text{ mA cm}^{-2}$ , GO/PEDOT-30 and GO/PEDOT-40 remain show the far higher areal capacitance than those of GO/PEDOT-10 and GO/PEDOT-20, but it is interesting that GO/PEDOT-30 reveals the longer discharge time and corresponding areal capacitance than those of GO/PEDOT-40, and then GO/PEDOT-30 composite films show the maximum capacitance of  $50 \text{ mF cm}^{-2}$  at  $5 \text{ mA cm}^{-2}$ . The GCD test results indicate the composite films prepared with moderate deposition time is more suitable for the fast charge/discharge, because short deposition time would lead to fewer electroactive materials loaded on the electrodes, while too long deposition time would cause too thick films which not facilitate the diffuse of ions from electrolyte within the composite films in the process of rapid charge/discharge.

To achieve further insight into the composite electrodes prepared with varying deposition time, EIS was performed and their Nyquist plots are shown in Fig. 6a. The impedance plots of four types of electrodes are featured by a vertical trend at low frequencies, which indicates the capacitive behavior according to the equivalent circuit theory [52], a semicircle at high frequency is not observed for the two types of electrodes, which is attributed to the

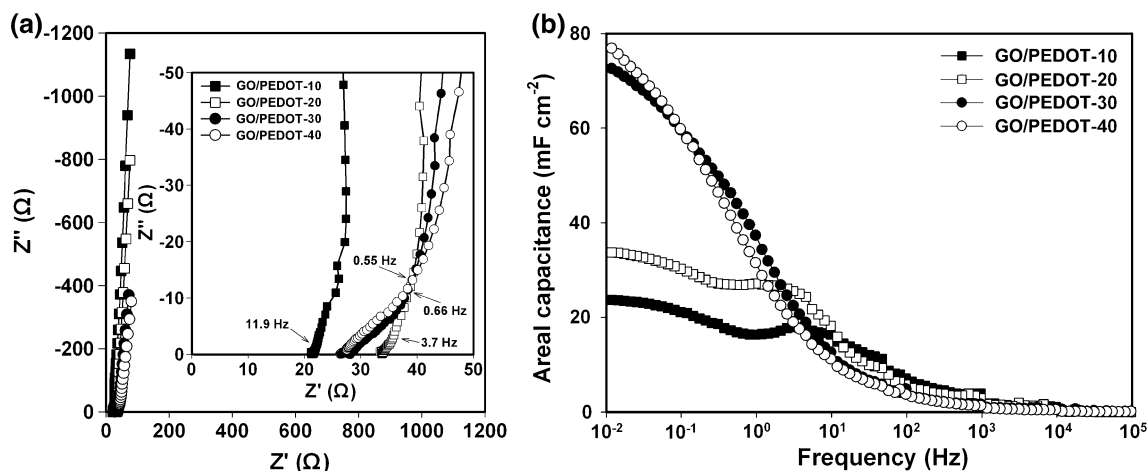


**Fig. 5** GCD curves of the super capacitor cells assembled by GO/PEDOT composite films electrodes with different deposition time at different GCD current densities

low interfacial charge-transfer resistance [40]. Another important parameter can be obtained at higher frequencies is the knee frequency ( $f_{knee}$ ), beyond which the capacitive behavior is replaced by the more inclined diffusion line, and higher knee frequency means faster charge transfer rates and lower diffusion impedance [52]. The  $f_{knee}$  is determined by the crossing of Warburg-type line (inclined  $45^\circ$ ) and low-frequency vertical line, it can be observed from the inset of Fig. 6a that knee frequencies of the four types of composite films in numerical order are GO/PEDOT-10 > GO/PEDOT-20 > GO/PEDOT-30 > GO/PEDOT-40, indicating thinner films possess faster charge transfer rates as a result of lower diffusion resistance of ions from electrolyte. The results manifest too much electroactive materials would result in larger diffusion resistance of electrolyte ions and increase electron transport resistance with the increase of loading amount, which are unfavourable for the rapid charge/discharge. Figure 6b presents the conversion capacitance obtained from EIS.

**Table 1** Discharge time and the corresponding areal capacitance obtained from the GCD curves at varying current densities for the supercapacitor cells assembled by GO/PEDOT composite films electrodes with different deposition time

Electrode	Discharge time at 0.5 mA cm <sup>-2</sup> /s	Areal capacitance at 0.5 mA cm <sup>-2</sup> /mF cm <sup>-2</sup>	Discharge time at 2 mA cm <sup>-2</sup>	Areal capacitance at 2 mA cm <sup>-2</sup> /mF cm <sup>-2</sup>	Discharge time at 5 mA cm <sup>-2</sup>	Areal capacitance at 5 mA cm <sup>-2</sup> /mF cm <sup>-2</sup>
GO/PEDOT-10	25.1	25.1	4.4	17.6	1.5	15
GO/PEDOT-20	36.3	36.3	7.9	31.6	2.4	24
GO/PEDOT-30	72.5	72.5	13.2	52.8	5.0	50
GO/PEDOT-40	83.8	83.8	16.8	67.2	4.6	46

**Fig. 6** **a** Nyquist plots of the super capacitor cells assembled by GO/PEDOT composite films electrodes with different deposition time, *inset* is the EIS in high-frequency region; **b** the relationship of areal capacitance with frequency for the four types of electrodes

The areal capacitance values of single composite films electrode can be obtained from the following Eq. (3) [53]:

$$C_s = -1/(\pi S f Z'') \quad (3)$$

Thereinto,  $C_s$  is the areal capacitance in  $F\text{ cm}^{-2}$ ,  $f$  the frequency in Hz,  $Z''$  the imaginary part of EIS in  $\Omega$ , and  $S$  the geometric surface area of active materials on single electrode ( $1\text{ cm}^2$  in this study). It can be seen from Fig. 6b that the areal capacitance increases as the adding of deposition time at the low-frequency region (0.01–0.1 Hz), With the frequency increases, GO/PEDOT-40 no longer exhibits the maximum capacitance, even GO/PEDOT-10 exhibits the relatively higher capacitance at the frequency range from 10 to 1 kHz. Compared with GO/PEDOT-40, we can also find that GO/PEDOT-30 films only have a lower capacitance at the low-frequency region, GO/PEDOT-30 shows the higher capacitance across the whole frequency range beyond 0.1 Hz. These results originated from the EIS characterization are in accord with the CV and GCD results.

### 3.4 Ragone plot and cyclic stability

The areal energy and power density are usually used for evaluating thin film micro-batteries because it has no

dependence for the comparison on the choice of other components including protective package and substrates [54]. The areal energy density and power density of the single composite films electrode can be obtained with the following Eqs. (4) and (5), respectively [38].

$$E = \frac{\frac{1}{2} C_s \Delta V^2}{3600} \quad (4)$$

$$P = \frac{3600E}{t} \quad (5)$$

Thereinto,  $E$  is the areal energy density in  $\text{Wh cm}^{-2}$ ,  $C_s$  the areal capacitance in  $F\text{ cm}^{-2}$ ,  $\Delta V$  the potential window (excluding  $iR$  drop) in V,  $P$  the areal power density in  $\text{W cm}^{-2}$  and  $t$  the discharge time in s. Since the GO/PEDOT-30 composite films electrodes with moderate deposition time show better performance for the fast charge/discharge, a Ragone plot of GO/PEDOT-30 electrode (Fig. 7a) is made according to the above Eqs. (4) and (5). We can see that the whole curves show a gradually smooth trend with the increase of GCD current density, indicating a superior rate capability. Furthermore, the GO/PEDOT composite films show an energy density of  $12.2\text{ }\mu\text{Wh cm}^{-2}$  at a power density of  $197.6\text{ }\mu\text{W cm}^{-2}$ , while it maintains  $4.47\text{ }\mu\text{Wh cm}^{-2}$  at  $3497\text{ }\mu\text{W cm}^{-2}$ ,

showing higher energy density and power density than those of the conducting polymers reported previously [38].

The cycle life is a crucial performance for the practical application of supercapacitor electrodes, the stability of the cells assembled by GO/PEDOT-30 composite films electrodes was evaluated using CV cycles at a scan rate of  $100 \text{ mV s}^{-1}$ , and an 20,000 cycles was performed. Figure 7b illustrates the results of the stability test, we can observe that the cycle tests for GO/PEDOT cause an increase in the capacitance up to 5000 cycles. It is possibly attributed to the surface wetting of the electrode caused by the cycle measurement [55, 56], which derives from the large electrochemical surface area of GO, leading to more available electroactive surface area with the cycles, and what's more, the GO/PEDOT films retain 96.6 % of the initial capacitance after 10,000 cycles, as well as persisting 90.1 % for 20,000 cycles, highlighting the ultralong electrochemical stability of the composite materials. It is well

known that conducting polymer usually suffers from a poor cyclic stability owing to the degradation caused by the swelling and shrinking of CPs [28, 57]. We consider that the improved stability can be ascribed to the robust support of GO nanosheets for the PEDOT, enhancing the mechanical strength of the composites and preventing the PEDOT from swelling and shrinking for the long cycles.

In general, the superior capacitive behavior and the ultralong cycle life shown by GO/PEDOT composite films can be attributed to the following reasons: (1) PEDOT-coated GO sheets form layer-within/on-layer intercalated composite nanostructures and the synergic effect between them. (2) The coatings of PEDOT on GO sheets prevent them from aggregating, leading to the improved electrical double-layer capacitance; (3) The composite films combine the advantages of EDLCs and redox supercapacitors originated from GO and PEDOT.

## 4 Conclusions

We have prepared the GO/PEDOT composite films electrodes with a facile and feasible electrochemical polymerization method. The obtained GO/PEDOT composites exhibited superior electrochemical properties and ultralong cycle life, achieving a high areal capacitance of  $66.3 \text{ mF cm}^{-2}$  at  $10 \text{ mV s}^{-1}$  CV scan and maintaining the 90.1 % of original capacitance after 20,000 CV cycles, which can be ascribed to the intercalated nanostructures and the synergistic effects between them. The loading amount of the composites on the electrodes could be easily tuned by changing the deposition time and the varying deposition time have a significant effect on their capacitive behavior, moderate deposition time is more suitable for the rapid charge/discharge. This facile and effective approach for the preparation of GO/PEDOT composite electrodes is very promising to be used for the high-performance electrochemical capacitors and can be easily transferred to conductive flexible substrate for future flexible devices.

**Acknowledgments** The author appreciates the funding from National Natural Science Foundation of China (21274082) and Shanxi Province (2015021079), China Postdoctoral Science Foundation funded Project (2015M571283), and the Scientific Research Start-up Funds of Shanxi University (203533801002).

## References

1. M. Acerce, D. Voiry, M. Chhowalla **10**, 313–318 (2015)
2. S. Kondrat, P. Wu, R. Qiao, A.A. Kornyshev, *Nat. Mater.* **13**, 387–393 (2014)
3. H.J. Tang, J.Y. Wang, H.J. Yin, H.J. Zhao, D. Wang, Z.Y. Tang, *Adv. Mater.* **27**, 1117–1123 (2015)
4. D. Vonlanthen, P. Lazarev, K.A. See, F. Wudl, A.J. Heeger, *Adv. Mater.* **26**, 5095–5100 (2014)

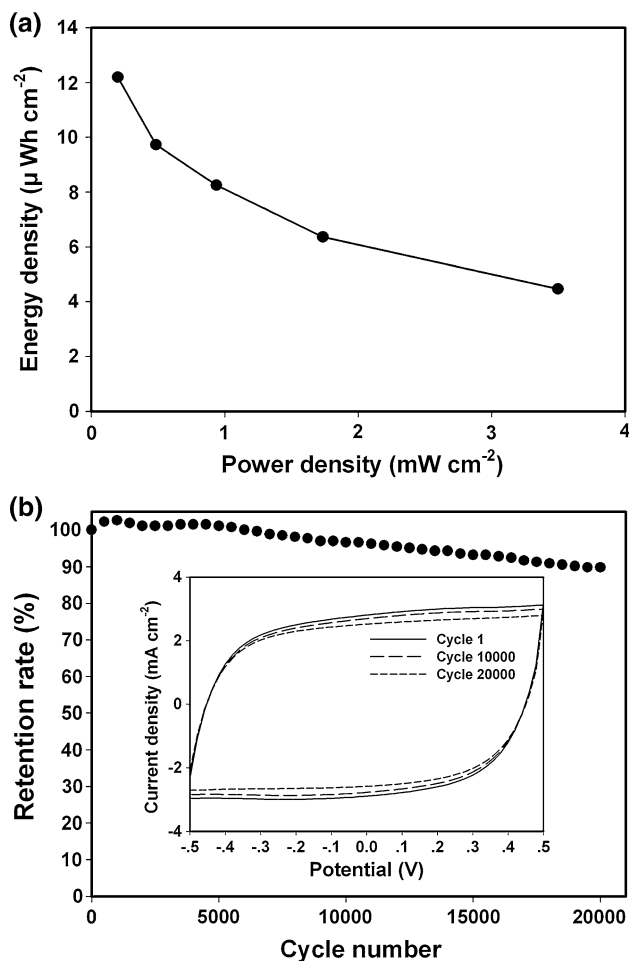


**Fig. 7** **a** Ragone plots of GO/PEDOT-30 composite films electrodes; **b** the relationship of capacitance retention rate and cycle number for GO/PEDOT-30 electrodes at  $100 \text{ mV s}^{-1}$  CV scan for 20,000 cycles, the inset is the corresponding cyclic voltammogram tested

5. W.J. Qian, F.X. Sun, Y.H. Xu, L.H. Qiu, C.H. Liu, S.D. Wang, F. Yan, *Energy Environ. Sci.* **7**, 379–386 (2014)
6. Lu. Wang, X. Feng, L.T. Ren, Q.H. Piao, J.Q. Zhong, Y.B. Wang, H.W. Li, Y.F. Chen, B. Wang, *J. Am. Chem. Soc.* **137**, 4920–4923 (2015)
7. H. Yue, H.H. Cheng, F. Zhao, N. Chen, L. Jiang, Z.H. Feng, L.T. Qu, *Nanoscale* **6**, 6448–6451 (2014)
8. X. Xiao, S. Li, H. Wei, D. Sun, Y. Wu, G. Jin, F. Wang, Y. Zou, *J. Mater. Sci. Mater. Electron.* **26**, 4226–4233 (2015)
9. H. Sunder, P. She, K.L. Xu, Y.X. Shang, S.Y. Yin, Z.N. Liu, *Synth. Met.* **209**, 68–73 (2015)
10. Q. Lu, J.G.G. Chen, J.Q. Xiao, *Angew. Chem. Int. Ed.* **52**, 1882–1889 (2013)
11. X.B. Liu, P.B. Shang, Y.B. Zhang, X.L. Wang, Z.M. Fan, B.X. Wang, Y.Y. Zheng, *J. Mater. Chem. A* **2**, 15273–15278 (2014)
12. F. Beguin, V. Presser, A. Balducci, E. Frackowiak, *Adv. Mater.* **26**, 2219–2251 (2014)
13. A.N. Naveen, P. Manimaran, S. Selladurai, *J. Mater. Sci. Mater. Electron.* (2015). doi:10.1007/s10854-015-3582-2
14. V. Augustyn, P. Simon, B. Dunn, *Energy Environ. Sci.* **7**, 1597–1614 (2014)
15. I. Shakir, Z. Ali, J. Bae, J. Park, D.J. Kang, *Nanoscale* **6**, 4125–4130 (2014)
16. L.L. Liu, Z.Q. Niu, L. Zhang, W.Y. Zhou, X.D. Chen, S.S. Xie, *Adv. Mater.* **26**, 4855–4862 (2014)
17. Z. Li, Z. Liu, D. Li, B. Li, Q. Li, Y. Huang, H. Wang, *J. Mater. Sci. Mater. Electron.* **26**, 353–359 (2015)
18. X.W. Ma, J.W. Liu, C.Y. Liang, X.W. Gong, R.C. Che, *J. Mater. Chem. A* **2**, 12692–12696 (2014)
19. Z. He, Y. Zhu, Z. Xing, Z. Wang, *J. Mater. Sci. Mater. Electron.* **26**, 5697–5702 (2015)
20. X.H. Lu, Y.X. Zeng, M.H. Yu, T. Zhai, C.L. Liang, S.L. Xie, M.S. Balogun, Y.X. Tong, *Adv. Mater.* **26**, 3148–3155 (2014)
21. J. Wei, S. Xing, B. Yan, D. He, H. Suo, C. Zhao, *J. Mater. Sci. Mater. Electron.* **26**, 4185–4192 (2015)
22. Y.W. Zhu, S. Murali, M.D. Stoller, K.J. Ganesh, W.W. Cai, P.J. Ferreira, A. Pirkle, R.M. Wallace, K.A. Cychosz, M. Thommes, D. Su, E.A. Stach, R.S. Ruoff, *Science* **332**, 1537–1541 (2011)
23. R. Liu, S.B. Lee, *J. Am. Chem. Soc.* **130**, 2942–2943 (2008)
24. C.H. Lei, P. Wilson, C. Lekakou, *J. Power Sources* **196**, 7823–7827 (2011)
25. D.R. Dreyer, S. Park, C.W. Bielawski, R.S. Ruoff, *Chem. Soc. Rev.* **39**, 228–240 (2010)
26. Z.F. Li, H.Y. Zhang, Q. Liu, Y.D. Liu, L. Stanciu, J. Xie, *Carbon* **71**, 257–267 (2014)
27. J. Li, H.Q. Xie, Y. Li, Fabrication of graphene oxide/polypyrrole nanowire composite for high performance supercapacitor electrodes. *J. Power Sources* **241**, 388–395 (2013)
28. S. Sahoo, S. Dhibar, G. Hatui, P. Bhattacharya, C.K. Das, *Polymer* **54**, 1033–1042 (2013)
29. A.R. Liu, C. Li, H. Bai, G.Q. Shi, *J. Phys. Chem. C* **114**, 22783–22789 (2010)
30. Q.Q. Zhou, Y.R. Li, L. Huang, C. Li, G.Q. Shi, *J. Mater. Chem. A* **2**, 17489–17494 (2014)
31. H.H. Chang, C.K. Chang, Y.C. Tsai, C.S. Liao, *Carbon* **50**, 2331–2336 (2012)
32. T. Lindfors, A. Osterholm, J. Kauppila, M. Pesonen, *Electrochim. Acta* **110**, 428–436 (2013)
33. Y.Y. Horng, Y.C. Lu, Y.K. Hsu, C.C. Chen, L.C. Chen, K.H. Chen, *J. Power Sources* **195**, 4418–4422 (2010)
34. J.P. Liu, J. Jiang, M. Bosman, H.J. Fan, *J. Mater. Chem.* **22**, 2419–2426 (2012)
35. Y.X. Xu, H. Bai, G.W. Lu, C. Li, G.Q. Shi, *J. Am. Chem. Soc.* **130**, 5856–5857 (2008)
36. Y.Z. Chang, G.Y. Han, M.Y. Li, F. Gao, *Carbon* **49**, 5158–5165 (2011)
37. L.Y. Yuan, B. Yao, B. Hu, K.F. Huo, W. Chen, J. Zhou, *Energy Environ. Sci.* **6**, 470–476 (2013)
38. H.G. Wei, J.H. Zhu, S.J. Wu, S.Y. Wei, Z.H. Guo, *Polymer* **54**, 1820–1831 (2013)
39. C.Z. Zhu, J.F. Zhai, D. Wen, S.J. Dong, *J. Mater. Chem.* **22**, 6300–6306 (2012)
40. Y.Q. Han, B. Ding, H. Tong, X.G. Zhang, *J. Appl. Polym. Sci.* **121**, 892–898 (2011)
41. H.J. Shin, S.S. Jeon, S.S. Im, *Synth. Met.* **161**, 1284–1288 (2011)
42. D.X. Han, G.F. Yang, J.X. Song, L. Niu, A. Ivaska, *J. Electroanal. Chem.* **602**, 24–28 (2007)
43. L. Chen, C.Z. Yuan, H. Dou, B. Gao, S.Y. Chen, X.G. Zhang, *Electrochim. Acta* **54**, 2335–2341 (2009)
44. H.L. Guo, X.F. Wang, Q.Y. Qian, F.B. Wang, X.H. Xia, *ACS Nano* **3**, 2653–2659 (2009)
45. Y.Z. Chang, G.Y. Han, J.P. Yuan, D.Y. Fu, F.F. Liu, S.D.A. Li, *J. Power Sources* **238**, 492–500 (2013)
46. F. Alvi, M.K. Ram, P.A. Basnayaka, E. Stefanakos, Y. Goswami, A. Kumar, *Electrochim. Acta* **56**, 9406–9412 (2011)
47. J.C. Meyer, A.K. Geim, M.I. Katsnelson, K.S. Novoselov, D. Obergfell, S. Roth, C. Girit, A. Zettl, *Solid State Commun.* **143**, 101–109 (2007)
48. K. Jurewicz, V.E. Frackowiak, F. Beguin, *Electrochim. Acta* **50**, 2499–2506 (2005)
49. G. Wallace, G. Spinks, *Soft Matter* **3**, 665–671 (2007)
50. H. Fang, S.C. Zhang, X.M. Wu, W.B. Liu, B.H. Wen, Z.J. Du, T. Jiang, *J. Power Sources* **235**, 95–104 (2013)
51. M. Yu, Y. Zeng, C. Zhang, X. Lu, C. Zeng, C. Yao, Y. Yang, Y. Tong, *Nanoscale* **5**, 10806–10810 (2013)
52. C. Peng, J. Jin, G.Z. Chen, *Electrochim. Acta* **53**, 525–537 (2007)
53. K.S. Ryu, Y.G. Lee, K.M. Kim, Y.J. Park, Y.S. Hong, X.L. Wu, M.G. Kang, N.G. Park, R.Y. Song, J.M. Ko, *Synth. Met.* **153**, 89–92 (2005)
54. N.J. Dudney, *Electrochem. Soc. Interface* **17**, 44 (2008)
55. H.L. Wang, C.M.B. Holt, Z. Li, X.H. Tan, B.S. Amirkhiz, Z.W. Xu, B.C. Olsen, T. Stephenson, D. Mitlin, *Nano Res.* **5**, 605–617 (2012)
56. Y.F. Xu, I. Hennig, D. Freyberg, A.J. Strudwick, M.G. Schwab, T. Weitz, K.C.P. Cha, *J. Power Sources* **248**, 483–488 (2014)
57. J.Y. Huang, K. Wang, Z.X. Wei, *J. Mater. Chem.* **20**, 1117–1121 (2010)